



**HAL**  
open science

## How does bending the uranyl unit influence its spectroscopy and luminescence

Hanna Oher, André Severo Pereira Gomes, Richard E. Wilson, David D. Schnaars, Valérie Vallet

► **To cite this version:**

Hanna Oher, André Severo Pereira Gomes, Richard E. Wilson, David D. Schnaars, Valérie Vallet. How does bending the uranyl unit influence its spectroscopy and luminescence. *Inorganic Chemistry*, 2023, 62, pp.9273–9284. 10.1021/acs.inorgchem.3c00847 . hal-04017334

**HAL Id: hal-04017334**

**<https://hal.science/hal-04017334>**

Submitted on 21 Jun 2023

**HAL** is a multi-disciplinary open access archive for the deposit and dissemination of scientific research documents, whether they are published or not. The documents may come from teaching and research institutions in France or abroad, or from public or private research centers.

L'archive ouverte pluridisciplinaire **HAL**, est destinée au dépôt et à la diffusion de documents scientifiques de niveau recherche, publiés ou non, émanant des établissements d'enseignement et de recherche français ou étrangers, des laboratoires publics ou privés.

# How does bending the uranyl unit influence its spectroscopy and luminescence

Hanna Oher,<sup>†</sup> André Severo Pereira Gomes,<sup>‡</sup> Richard E. Wilson,<sup>\*,¶</sup> David D. Schnaars,<sup>¶</sup> and Valérie Vallet<sup>\*,‡</sup>

<sup>†</sup>*Univ. Rennes, CNRS, ISCR (Institut des Sciences Chimiques de Rennes) – UMR 6226, F-35000 Rennes, France*

<sup>‡</sup>*Univ. Lille, CNRS, UMR 8523 - PhLAM - Physique des Lasers Atomes et Molécules, F-59000 Lille, France*

<sup>¶</sup>*Chemical Sciences and Engineering Division, Argonne National Laboratory, Lemont, Illinois 60439, United States*

E-mail: rewilson@anl.gov; valerie.vallet@univ-lille.fr

## Abstract

Bent uranyl complexes can be formed with chloride ligands and 1,10-phenanthroline (phen) ligands bound to the equatorial and axial planes of the uranyl(VI) moiety, as revealed by the crystal structures, IR and Raman spectroscopy and quantum chemical calculations. With the goal of probing the influence of chloride and phenanthroline coordination enforcing the bending on the absorption and emission spectra of this complex, spin-orbit time-dependent density functional theory calculations for the bare uranyl complexes as well as for the free  $\text{UO}_2\text{Cl}_2$  subunit and the  $\text{UO}_2\text{Cl}_2(\text{phen})_2$  complex were performed. The emission spectra have been fully simulated by ab initio methods and compared to experimental photoluminescence spectra, recorded for the first time for  $\text{UO}_2\text{Cl}_2(\text{phen})_2$ . Notably, the bending of uranyl in  $\text{UO}_2\text{Cl}_2$  and

$\text{UO}_2\text{Cl}_2(\text{phen})_2$  triggers excitations of the uranyl bending mode, yielding a denser luminescence spectrum.

## Introduction

The uranyl ion,  $\text{UO}_2^{2+}$ , on account of its high chemical stability, is ubiquitous in uranium chemistry. Up to a few years ago, the uranyl subunit had been characterized essentially as a linear trans-oxo unit, with very few structures exhibiting  $\text{O}_{\text{yl}}-\text{U}-\text{O}_{\text{yl}}$  bond angles deviating (by few degrees) from linearity.<sup>1,2</sup> The underlying cause for the predominance of linear  $\text{O}_{\text{yl}}-\text{U}-\text{O}_{\text{yl}}$  bonds in  $\text{UO}_2^{2+}$  is the notable participation of the U 5f and 6p orbitals in the  $\text{U}-\text{O}_{\text{yl}}$  bond, while in the iso-electronic  $\text{ThO}_2$  molecule 6d and 5f orbitals hybridize and favor a bent geometry.<sup>3,4</sup> Hratchian *et al.*<sup>5</sup> and Schreckenbach *et al.*<sup>6,7</sup> however proposed the existence of stable “cis-uranyl” structures in uranyl dihydroxides and tetracoordinated  $[\text{UO}_2\text{X}_4]^{2-}$  (X = F, Cl, and OH) complexes, with  $\text{O}_{\text{yl}}-\text{U}-\text{O}_{\text{yl}}$  bond angles as acute as  $100^\circ$ . In both linear and bent structures, the “yl” oxygen atoms carry negative charges making them Lewis bases, with a basicity that increases pairwise with yl-bond weakening as stronger Lewis basis are coordinated in the uranyl equatorial plane.<sup>8,9</sup>

There have been several attempts to synthesize bent actinyl complexes. A simple synthetic route was proposed by Schöne *et al.*<sup>10</sup>, in which simply dropping 1,10-phenanthroline (phen) into a uranyl chloride solution in acetone forms the  $\text{UO}_2\text{Cl}_2(\text{phen})_2$  complex, in which the uranyl group is strongly bent ( $161.8(1)^\circ$ ), and consequently the equatorial plane is broken up. Langer *et al.*<sup>11</sup> also showed that applying physical pressure on the uranyl-sulfate system can result in a uranyl oxo-salt phase holding a considerably bent uranyl. In 2018, Hayton catalogued the uranyl complexes that feature a  $\text{O}_{\text{yl}}-\text{U}-\text{O}_{\text{yl}}$  angle smaller than  $172^\circ$ ,<sup>2</sup> to which we must add the works by Carter *et al.*<sup>12</sup> and Carter *et al.*<sup>13</sup>.

In this work, the focus is on the impact of bending on the uranyl electronic structure. Indeed the ligand induced weakening of uranyl internal bond is expected to impact the elec-

tronic structures and optical properties of uranyl(VI) complexes. From the detailed work of Zhang and Pitzer<sup>14</sup> on the theoretical side and Denning on the experimental side,<sup>15,16</sup> the spectra of linear uranyl can be explained in terms of excitations from the “yl-bonding” orbitals ( $\sigma_u$ ,  $\sigma_g$ ,  $\pi_u$ ,  $\sigma_g$ ), to the uranium centered nonbonding  $5f_\delta$ , and  $5f_\phi$  orbitals. Typically the spectrum between 20 000 and 32 500  $\text{cm}^{-1}$  arises from two, parity conserving orbital excitations,  $\sigma_u \rightarrow 5f_\delta$  and  $\sigma_u \rightarrow 5f_\phi$ , superimposed with vibrational fine structures. While these excited configurations (abbreviated as  $\sigma_u\delta$  and  $\sigma_u\phi$ ) only weakly depend on the nature of the equatorial ligands, they do give rise to numerous excited states due to three perturbations of similar magnitudes : the equatorial ligand field, spin-orbit coupling (SOC) and electron correlation. The various relativistic correlated calculations on the bare uranyl ion reported so far reveal the interplay between SOC and electron correlation, as both the choice of the relativistic framework (four-component, two-component with SOC treated, or two-step relativistic methods), and the treatment of electron correlation via wavefunction theory (WFT) or density functional theory (DFT), may change the relative ordering of the low-lying excited states. These parameters in the calculations also affect the spectroscopic character the lowest state, responsible for the observed luminescence with a long lifetime; it is found to be either a  $1_g$  state (arising from the  ${}^3\Delta_g$  spin-free (SF) triplet state)<sup>14,17,18</sup> or a  $2_g$  state (with a dominant  ${}^3\Phi_g$  character),<sup>18-23</sup> the difference between the various SOC states being small (a few hundred wavenumbers if not less), highlighting how challenging the electronic structure of actinide complexes is.<sup>24-26</sup>

Several theoretical studies investigated the characters of the low-lying excited states of uranyl complexed with water,<sup>27,28</sup> halides<sup>19,23,29-31</sup> or acetone ligands,<sup>29</sup> revealing that ligand-field splitting induced by the equatorially bound ligands competes with SOC and electron correlation. This work aims at pushing further the discussion of the impact of structural changes on uranyl spectroscopic properties, by considering the effect of bending the  $\text{O}_{y1}-\text{U}-\text{O}_{y1}$  unit, taking the structure of the uranylbis(1,10-phenanthroline) complex shown in Figure 1,  $\text{UO}_2\text{Cl}_2(\text{phen})_2$  originally synthesized by Schöne *et al.*<sup>10</sup>, which features

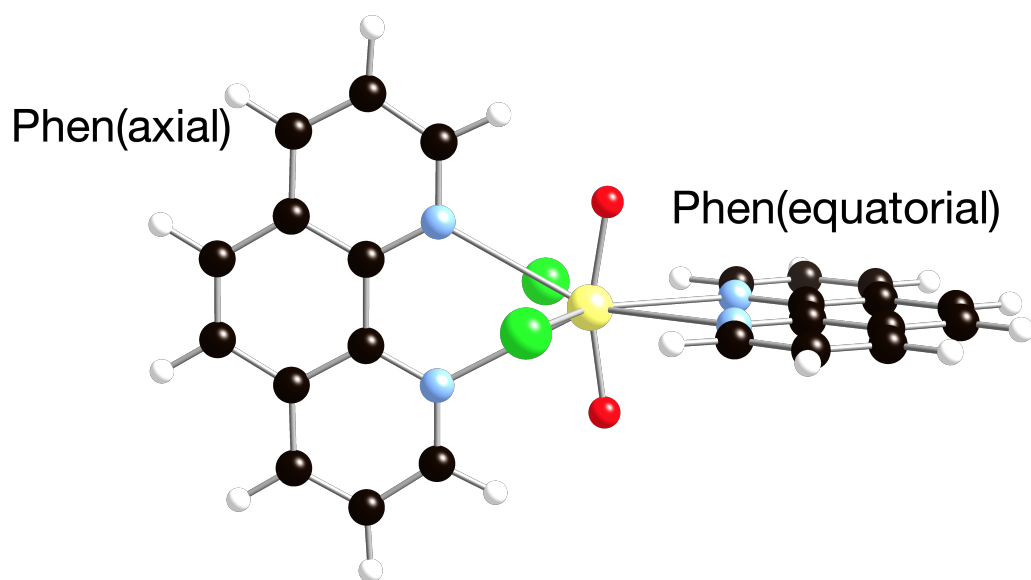


Figure 1: Perspective view of the  $\text{UO}_2\text{Cl}_2(\text{phen})_2$  bent uranyl complex. Color code: yellow (U), red (O), light blue (N), black (C), white (H).

a significantly distorted  $O_{yl}-U-O_{yl}$  angle ( $161.8(1)^\circ$ ).

In this study, we use quantum chemical (QC) methods to easily explore different structural models for the system - bent- $UO_2^{2+}$ ,  $UO_2Cl_2$ ,  $UO_2Cl_2(\text{phen})$  and  $UO_2Cl_2(\text{phen})_2$  - corresponding to a decomposition of the  $UO_2Cl_2(\text{phen})_2$  complexes into subunits, and from that assess the relative influence of individual ligand groups (chlorine and phenanthroline groups) on the degree of bending and in the electronic spectrum, as well as to quantify the ligand-field effects of the chlorines and the axially and equatorially bound phenanthroline groups, and their importance to the nature of the low-lying excited states. The computational data are compared to experimental luminescence and vibrational spectroscopic data collected on  $UO_2Cl_2(\text{phen})_2$  that was synthesized by an alternative method to that previously reported by Schöne *et al.*<sup>10</sup>.

## Computational Details

The geometry optimizations of the  $UO_2Cl_2(\text{phen})_2$  complex in its ground state (singlet state) and its lowest excited triplet state were carried out with the Gaussian 16 software,<sup>32</sup> in the gas phase using density functional theory (DFT) with the PBE0 functional<sup>33,34</sup> and the D3 dispersion correction with Becke damping to account for non-covalent interactions,<sup>35,36</sup> which turned out to be important to obtain interatomic uranyl-ligand bond distances matching the experimental data within about  $0.03 \text{ \AA}$  (see also Table S1). Note that all calculations (geometry optimizations and calculations of absorption and emission energies) were performed in the gas-phase, with arguments detailed in 1 of the Supporting Information. In addition to that, we performed optimizations on its subunits  $UO_2Cl_2$ ,  $UO_2Cl_2(\text{phen})_{ax}$ , and  $UO_2Cl_2(\text{phen})_{eq}$ . For all complexes, two configurations for the O-U-O bond angle were investigated: one in which it was allowed to relax and another where it was constrained to be equal to  $180^\circ$ . In the latter cases, one imaginary vibrational mode corresponding to the bending of the uranyl moiety always appeared confirming that the linear geometries are transition-state

structures that relax to bent structures when the linearity constraint is lifted. The U atom was described using a small core relativistic pseudopotential (60 core electrons)<sup>37</sup> with the corresponding segmented basis set including 3g polarization functions;<sup>38,39</sup> all other atoms were described with def2-TZVP basis sets.<sup>40</sup> To determine the energy cost of bending we also used the single-reference MP2 post-Hartree-Fock method to perform single-point calculations at the PBE0-D3 optimized geometries. Note that uranyl complexes are expected to have marginal multireference character,<sup>21</sup> and that MP2 is expected to yield more accurate relative energies than any functional of the density (see Table S2 and discussions in refs 41–43). In these MP2 calculations the core orbitals were frozen, namely the 1s orbitals of first row elements, the 1s, 2s, and 2p of chlorine atoms, and the 5s, 5p, and 5d pseudovalence orbitals of uranium.

Uranium–ligand chemical bonds were analyzed through the topology of the electronic density with the QTAIM theory<sup>44,45</sup> as implemented in the AIMAll package.<sup>46</sup> Natural population analysis and Wiberg bond order were computed with the NBO 7 program.<sup>47</sup>

To investigate how the bending of the uranyl moiety influences the energy position and nature of low-lying excited states of  $\text{UO}_2\text{Cl}_2(\text{phen})_2$ , we chose a computationally affordable yet reliable approach, namely using time-dependent DFT (TDDFT) combined with the range-separated hybrid CAM-B3LYP functional,<sup>48</sup> as it has proven to be more reliable than other hybrid functionals for the absorption and emission energies of small to large uranyl(VI) complexes,<sup>20,21,49–54</sup> including simulations of core-energy levels.<sup>55</sup> The ADF program<sup>56–58</sup> was used for all TDDFT calculations with the full (non-ALDA) kernel, and the lowest 16 electronic states were computed. Calculations are performed in the gas phase for the linear and bent uranyl complexes. Relativistic effects were included via either the scalar relativistic (SR) or spin-orbit (SO) ZORA Hamiltonians.<sup>59–61</sup> We employed basis sets of triple- $\zeta$  plus polarization (TZ2P) quality for all atoms without freezing core orbitals.<sup>62</sup>

The theoretical vibronic progressions of the  $\text{UO}_2\text{Cl}_2$ ,  $\text{UO}_2\text{Cl}_4^{2-}$  and  $\text{UO}_2\text{Cl}_2(\text{phen})_2$  luminescence were computed with the ezSpectrum 3.0<sup>63</sup> software. The Franck-Condon factors

(FCFs) were obtained based on the structures and the full set of vibrational modes of the ground and first low-lying excited state structures of complexes of interest following the methodology deduced previously and reported elsewhere.<sup>51-53</sup> The first low-lying excited state structures were obtained using the TDDFT method as implemented in Gaussian 16<sup>32</sup> using the same PBE0-D3 functional as for the ground-state description. The temperature for the FCF calculations was set to repeat the experimental conditions, namely, 4 K for  $\text{UO}_2\text{Cl}_2$ <sup>64</sup> and 80 K for  $\text{UO}_2\text{Cl}_4^{2-}$  and  $\text{UO}_2\text{Cl}_2(\text{phen})_2$  complexes. For the simplicity of the experimental luminescence spectra assignments, the second set of calculations was performed at 4 K to minimize the contributions from the thermally active vibrational modes.

## Experimental Details

*CAUTION!* <sup>238</sup>U, is an  $\alpha$ -emitting radionuclide. This material was handled in a radiological facility under radiological controls All reactions were conducted under ambient atmospheric conditions except where noted. All materials were used as received from commercial sources. KBr was ground and dried for a minimum of 48 h at 120 °C.  $(\text{Ph}_4\text{P})_2\text{UO}_2\text{Cl}_4 \cdot 2\text{MeCN}$ , was synthesized as described previously,<sup>65</sup> and washed three times with 200  $\mu\text{L}$  of  $\text{H}_2\text{O}$  to remove residual HCl.

## Synthesis

In a 2 mL shell vial, 30.6 mg (0.026 mmol) of  $(\text{Ph}_4\text{P})_2\text{UO}_2\text{Cl}_4 \cdot 2\text{MeCN}$  was dissolved in 750  $\mu\text{L}$  of MeCN forming a yellow-green solution, to which was added 500  $\mu\text{L}$  of MeCN containing 31.0 mg (0.156 mmol, 6 equiv) of 1,10-phenanthroline- $\text{H}_2\text{O}$  without color change. This solution was warmed in a water bath at 50 °C and allowed to cool slowly to room temperature resulting in the deposition of yellow-green single crystals (9.8 mg, 54 % yield). For isotopic exchange of the  $\text{O}_{\text{yl}}$  atoms to aid in spectral assignment of the vibrational structure, <sup>18</sup>O labeled water was used in the preparation of the  $(\text{Ph}_4\text{P})_2\text{UO}_2\text{Cl}_4 \cdot 2\text{MeCN}$

starting material. Prior to crystallization, the capped sample was irradiated under UV light to facilitate uranyl-oxo ligand exchange with the  $^{18}\text{O}$  water. This salt was used in subsequent synthesis of the labeled  $\text{UO}_2\text{Cl}_2(\text{phen})_2$  complex.  $\text{Cs}_2\text{UO}_2\text{Cl}_4$  was prepared according to literature methods.<sup>66</sup>

## X-ray Crystallography

Single crystal X-ray diffraction data were collected using a Bruker APEX II diffractometer and detector with a Quazar Microfocus source,  $\text{Mo}_{K\alpha}$  radiation. Single crystals were affixed to a fine glass capillary using a quick drying epoxy. Data were collected at 100 K using an Oxford Cryosystems Cryostream 700 device. Data were corrected for absorption using SADABS,<sup>67</sup> structures were solved using SHELXS and refined with SHELXL.<sup>68</sup> The crystallographic data including the structure factors have been deposited with the Cambridge Crystallographic Data Centre under accession code 2245382.

## Spectroscopy

FT-IR spectra were collected on pressed pellets containing 1-5 wt% loading of the sample diluted into dry KBr powder using a Nicolet 870 FT-IR spectrometer. Data were collected as an average of 16 scans over  $4000 - 400 \text{ cm}^{-1}$  with a resolution of  $2 \text{ cm}^{-1}$ . Raman data were collected from randomly oriented single crystals using circularly polarized 785 nm laser light on a Renishaw inVia Raman microscope system. The FT-IR and Raman spectra of the complexes are presented in the Figure S1 and Figure S2).

Photoluminescence of the uranyl salts  $\text{Cs}_2\text{UO}_2\text{Cl}_4$  and  $\text{UO}_2\text{Cl}_2(\text{phen})_2$  was collected using the 442 nm ( $22\,624 \text{ cm}^{-1}$ ) excitation line of a He-Cd laser on the Renishaw inVia Raman microscope. Emission was collected on randomly oriented single crystals using circularly polarized radiation with a defocused and attenuated laser beam to prevent sample burning and detector saturation. The emission wavelengths were recorded from 100 to  $8000 \text{ cm}^{-1}$  lower in frequency relative the excitation wavelength at 293 K and 80 K. Samples were

mounted on custom tantalum crucibles to which a glass coverslip had been epoxied. The temperature was thermostated using a Linkham 600 series sample stage with flowing liquid nitrogen.

## Results and Discussion

### Synthesis and Crystallographic Structure

Prior reports of uranyl molecules whose  $\text{O}\equiv\text{U}\equiv\text{O}$  bond angle deviates significantly from linearity are known in the literature.<sup>2,10,12,13</sup> The synthesis reported here was conducted independently exploiting the  $(\text{Ph}_4\text{P})_2\text{UO}_2\text{Cl}_4\cdot 2\text{MeCN}$  salts and their solvates, reported previously,<sup>65</sup> as starting materials in warm MeCN solutions under ambient conditions with an excess of 1,10-phenanthroline. Prior synthetic reports employed alternate solvents, e.g. acetone, hydrothermal aqueous methods and carboxylic acids in the presence of 1,10-phenanthroline to arrive at bent actinyl geometries, thus highlighting the potential richness of the synthetic phase space of these distorted -yl units.

Results of the X-ray crystallographic refinements shown in Table 1 demonstrate that the  $\text{UO}_2\text{Cl}_2(\text{phen})_2$  complex reported here is isostructural with that previously reported. Table 1 also presents the experimentally measured bond distances and angles for the reported complex.

### Structure and Bonding in $\text{UO}_2\text{Cl}_2(\text{phen})_2$

The geometry optimization of the  $\text{UO}_2\text{Cl}_2(\text{phen})_2$  molecule in the gas phase (DFT-PBE0-D3) converges to a bent molecule (See Table 2), with U-Cl bond distances perfectly matching the experimental values; the U-N bonds are slightly longer by 0.03 Å than in the crystal structure. The  $\text{O}\equiv\text{U}\equiv\text{O}$  angle is computed to be as bent ( $162.7^\circ$ ) as in the crystal ( $161.7^\circ$ ). This indicates that the significant bending of the  $\text{O}\equiv\text{U}\equiv\text{O}$  unit is not induced by the crystal packing but rather by the first coordination sphere. Phenanthroline preferably binds  $\text{UO}_2\text{Cl}_2$

Table 1: Crystallographic parameters and experimentally measured bond lengths (Å) and angles (deg) for  $\text{UO}_2\text{Cl}_2(\text{phen})_2$  from the single crystal X-ray diffraction refinements.

Crystallographic Parameters	
empirical formula	$\text{C}_{24}\text{H}_{16}\text{Cl}_2\text{N}_4\text{O}_2\text{U}$
formula weight ( $\text{g mol}^{-1}$ )	701.34
crystal habit	prismatic
color	yellow
size (mm)	0.12 x 0.07 x 0.06
crystal system	triclinic
space group	$P\bar{1}$
$V$ ( $\text{Å}^3$ )	1095.85(14)
$a$ (Å)	8.5359(6)
$b$ (Å)	9.4193(7)
$c$ (Å)	14.5821(11)
$\alpha$ (deg)	79.9640(10)
$\beta$ (deg)	89.7740(10)
$\gamma$ (deg)	71.9100(10)
$Z$	2
$T$ (K)	100
$\rho$ ( $\text{g cm}^{-3}$ )	2.125
$\mu$ ( $\text{mm}^{-1}$ )	7.681
GoF	1.017
$R_1$	0.0369
$wR^2$	0.0583

Bond lengths (Å) and angles (deg)			
$\text{U}\equiv\text{O}$	$\text{O}\equiv\text{U}\equiv\text{O}$	U-Cl	U-N
1.773(3)	161.71(11)	2.6634(9)	2.647(3)
1.780(3)		2.6846(9)	2.668(3)
			2.755(3)
			2.767(3)

Table 2: Symmetric ( $\nu_s$ ) and Asymmetric ( $\nu_{as}$ ) Vibrational Modes of the Uranyl Ions (in  $\text{cm}^{-1}$ ), Bond Length (in Å) and Angles (in deg) for  $\text{UO}_2\text{Cl}_2(\text{phen})_2$  and the Subunits  $\text{UO}_2\text{Cl}_2$ ,  $\text{UO}_2\text{Cl}_2(\text{phen})_{\text{ax}}$ , and  $\text{UO}_2\text{Cl}_2(\text{phen})_{\text{eq}}$  Optimized at the DFT-PBE0-D3 Level of Theory. MP2 Electronic Energy Differences between the Linear and (More Stable) Bent Structures ( $\Delta E$ , in  $\text{kJ mol}^{-1}$ ).

complex	geometry	$\nu_s$	$\nu_{as}$	U≡O	O≡U≡O	U-Cl	U-N <sub>ax</sub>	U-N <sub>eq</sub>	$\Delta E$
UO <sub>2</sub> Cl <sub>2</sub>	bent	949	1021	1.733	169.2	2.510(3)	-	-	0.0
	linear <sup>a</sup>	959	1032	1.729	180.0	2.514	-	-	8.7
UO <sub>2</sub> Cl <sub>2</sub> (phen) <sub>ax</sub>	bent	898	966	1.751	153.1	2.649	2.718	-	0.0
	linear <sup>a</sup>	936	1006	1.735	180.0	2.553	2.975	-	24.0
UO <sub>2</sub> Cl <sub>2</sub> (phen) <sub>eq</sub>	bent	933	1003	1.741	173.5	2.602	-	2.584	0.0
	linear <sup>a</sup>	936	1007	1.740	180.0	2.606	-	2.588	1.1
UO <sub>2</sub> Cl <sub>2</sub> (phen) <sub>2</sub>	crystal	820	890	1.778(3)	161.7	2.67(1)	2.759(5)	2.65(1)	
	bent	896	957	1.754	162.7	2.660	2.789	2.680	0.0
	linear <sup>a</sup>	918	988	1.743	180.0	2.651	3.004	2.669	33.5

<sup>a</sup> O≡U≡O angle constrained to 180°; one imaginary mode corresponding to the bending of the uranyl moiety.

in the equatorial position (See binding energies in Table S3 of the SI). However the axial phenanthroline group is the one that induces a significant bending. If the uranyl unit is forced to be linear, the bond distances to the chlorides and the “equatorial” phenanthroline group are unchanged, while the “axial” phenanthroline group that lie in the same plane as the yl-oxygen is pushed away at distances of 3.02 Å. From Table S3 this severe geometrical change corresponds to an energy gain of 33.5  $\text{kJ mol}^{-1}$  in agreement with the value 29.8  $\text{kJ mol}^{-1}$  reported by Schöne *et al.*<sup>10</sup>

Interestingly the optimal geometries of all subunits  $\text{UO}_2\text{Cl}_2$ ,  $\text{UO}_2\text{Cl}_2(\text{phen})_{\text{ax}}$ , and  $\text{UO}_2\text{Cl}_2(\text{phen})_{\text{eq}}$  also lead to a bent uranyl. The largest distortion from linearity is found for  $\text{UO}_2\text{Cl}_2(\text{phen})_{\text{ax}}$ , with an angle of 153.1°, paired with a significant energy stabilization upon bending, 24.0  $\text{kJ mol}^{-1}$ , almost as large as in the biphen complex. The computed symmetric and asymmetric vibrational frequencies of  $\text{UO}_2\text{Cl}_2(\text{phen})_2$  are larger than the experimental values, but the split between the two 62  $\text{cm}^{-1}$ , agrees with the value of 70  $\text{cm}^{-1}$  reported experimentally.

To investigate further the U≡O<sub>y1</sub> chemical bond and its changes as it bends, we have

applied the quantum theory of atoms-in-molecules (QTAIM), which probes the density at the bond critical points (BCPs) between pairs of atoms that are bonded to one another. One can classify the type of chemical bonding by the density properties at the BCP, namely, the value of the density  $\rho$ , the sign of the Laplacian  $\nabla^2\rho$  and the energy density  $H$ , and the comparison of the ratio between the potential energy density and the kinetic energy density at the BCP ( $|V|/G$ ) to 1, all of which are listed in Table S4, together with the delocalization index  $\delta(\text{U}, \text{L})$  and the Wiberg bond order, both of which measure the U–L bond order. In the stable  $\text{UO}_2\text{Cl}_2(\text{phen})_2$  bent geometry, the BCP parameters of the interactions between uranium and both the chlorides and the phenanthroline groups are very close to those reported by Vallet *et al.*<sup>8</sup> for  $\text{UO}_2\text{F}_4^{2-}$  and  $\text{UO}_2\text{Cl}_4^{2-}$  complexes, thus corresponding to ionic interactions. However for both equatorial bonds, the ( $|V|/G$ ) ration is larger than 1. With this we can qualify both U–N and U–Cl bonds as mostly ionic with some covalency, the latter being somewhat more covalent than the former both from the  $|V|/G$  ratio values and the bond-order values.

The  $\text{U}\equiv\text{O}_{\text{yl}}$  BCP characteristics  $\rho$ ,  $\nabla^2\rho$ , and  $H$ , and the bond orders are slightly smaller in the bent structures than in the linear ones, indicating a corresponding reduction of the strength of the  $\text{U}\equiv\text{O}_{\text{yl}}$  upon bending in line with a bond lengthening of 0.01 Å. The natural population analysis also points out that the population of the uranium 6d orbitals increases while that of the 5f orbitals decreases in the bent structure compared to the linear molecule. This is expected as 6d orbitals take a more prominent role in bonding for bent molecules such as  $\text{ThO}_2$ ,<sup>3,69</sup> and transition metal Mo(VI) and W(VI) oxides.<sup>70</sup> We stress though that the changes in the  $\text{U}\equiv\text{O}_{\text{yl}}$  bond upon bending are marginal, thus suggesting that the bending is mostly induced by the electrostatic repulsion of both the chloride and phenanthroline ligands.

Table 3: SO-TDDFT/CAM-B3LYP Vertical Transition Energies ( $\Delta E$ , in  $\text{cm}^{-1}$ ) in Linear  $\text{UO}_2^{2+}$  and Bent  $\text{UO}_2^{2+}$  (Computed at the  $\text{UO}_2\text{Cl}_2(\text{phen})_2$  PBE0-D3 Geometries) and  $\text{UO}_2\text{Cl}_4^{2-}$  Computed at the Crystal Geometry along with Experimental Data for  $\text{Cs}_2\text{UO}_2\text{Cl}_4$ .<sup>15,16</sup>

linear $\text{UO}_2^{2+}$ ( $r(\text{U}-\text{O}_{yl})=1.754 \text{ \AA}$ )		bent $\text{UO}_2^{2+}$ ( $r(\text{U}-\text{O}_{yl})=1.743 \text{ \AA}$ )	
transitions	$\Delta E$	transitions	$\Delta E$
$\sigma_u \rightarrow \phi$	14 097	$\sigma_u \rightarrow \phi$	13 500
$\sigma_u \rightarrow \phi$	15 447	$\sigma_u \rightarrow \phi$	14 801
$\sigma_u \rightarrow \delta$	17 007	$\sigma_u \rightarrow \delta$	16 572
$\sigma_u \rightarrow \delta$	18 892	$\sigma_u \rightarrow \delta$	18 451
$\sigma_u \rightarrow \phi$	20 738	$\sigma_u \rightarrow \phi$	20 117
$\sigma_u \rightarrow \delta(78\%) + \phi(18\%)$	22 007	$\sigma_u \rightarrow \delta(74\%) + \phi(21\%)$	21 541
$\sigma_u \rightarrow \phi(80\%) + \delta(16\%)$	24 002	$\sigma_u \rightarrow \phi(76\%) + \delta(19\%)$	23 212
$\pi_u \rightarrow \phi$	27 645	$\pi_u \rightarrow \phi$	26 480

$\text{UO}_2\text{Cl}_4^{2-}$			
transitions	$\Delta E$	$\Delta E^{exp}$	$\Delta\Delta E$
$\sigma_u(54\%) + \text{Cl}(39\%) \rightarrow \delta(82\%) + \phi(11\%)$	19 553	20 096	-543
$\sigma_u(54\%) + \text{Cl}(39\%) \rightarrow \delta(84\%) + \phi(11\%)$	19 553	20 097	-544
$\sigma_u(55\%) + \text{Cl}(47\%) \rightarrow \phi(69\%) + \delta(21\%)$	19 880	20 407	-527
$\sigma_u(57\%) + \text{Cl}(36\%) \rightarrow \phi(60\%) + \delta(32\%)$	20 578	21 316	-738
$\sigma_u(58\%) + \text{Cl}(34\%) \rightarrow \phi(72\%) + \delta(11\%)$	21 528	22 026	-498
$\sigma_u(57\%) + \text{Cl}(34\%) \rightarrow \phi(72\%) + \delta(11\%)$	21 596	22 076	-480
$\sigma_u(58\%) + \text{Cl}(36\%) \rightarrow \phi(45\%) + \delta(45\%)$	22 149	22 406	-257
$\sigma_u(59\%) + \text{Cl}(35\%) \rightarrow \delta(54\%) + \phi(26\%)$	22 334	22 750	-416

## Nature of the Low-Lying Electronic States of $\text{UO}_2\text{Cl}_2(\text{phen})_2$

The low-lying excited states of uranyl complexes are dominated by excitations out of the  $\sigma_u$   $\text{U}\equiv\text{O}$  bonding orbital (label referring to the linear  $\text{UO}_2^{2+}$  unit in the scalar relativistic framework) into the uranium centered nonbonding orbitals labeled  $\phi$ , and  $\delta$ . The lowest lying luminescent state can either have a  $(\sigma_u\delta)$  or  $(\sigma_u\phi)$  character, depending on how ligand-field affects the orbitals involved in the excitation. In the cases of  $\text{UO}_2\text{F}_2$ ,<sup>28</sup> and  $[\text{UO}_2\text{Cl}_3]^-$ <sup>71</sup> and the uranyl tetrahalides,<sup>31,72</sup> the luminescent state has a  $(\sigma_u\delta)$  character. To check whether our choice of basis sets and DFT functional (CAM-B3LYP) reproduces that known observation, we have computed the spectrum of  $\text{UO}_2\text{Cl}_4^{2-}$  using the crystal structure of  $[\text{PPh}_4]_2\text{UO}_2\text{Cl}_4 \cdot 2\text{MeCN}$ .<sup>65</sup> The assignment of the computed transition energies (See Table 3) does agree with the fact that the luminescent state corresponds to an excitation to a  $\delta$  orbital, noting that the excitation involves in almost equal amounts the  $\sigma_u$  uranyl orbital and the chloride 3p orbitals. It is also noteworthy the excellent agreement between the computed transition energies and experimental data for  $\text{UO}_2\text{Cl}_4^{2-}$  as noted previously by Gomes *et al.*<sup>31</sup> for the same system and by Tecmer *et al.*<sup>50</sup> and Oher *et al.*<sup>51-53</sup> for other uranyl complexes. We shall here remark that the onset of valence excitation energies for  $\text{UO}_2^{2+}$  appears several thousands wavenumbers lower than in  $\text{UO}_2\text{Cl}_4^{2-}$ . As noted earlier, for  $\text{UO}_2^{2+}$ , TDDFT (CAM-B3LYP), in comparison to wavefunction methods, places the first excited states at lower energies than complete active space second-order perturbation theory (CASPT2) and intermediate Hamiltonian Fock-space coupled cluster (IHFSCC) methods.<sup>21</sup> The origin of these differences between the two methods has not been elucidated and calls for further investigations for the bare uranyl itself and for the “small”  $\text{UO}_2\text{Cl}_2$  molecule, as it may induce a bias in the emission energy of the  $\text{UO}_2\text{Cl}_2$ , as discussed later.

Prior to discussing the nature of the low-lying electronic states in the system of interest,  $\text{UO}_2\text{Cl}_2(\text{phen})_2$ , we wish to quantify in a systematic way the relative importance various effects, such as 1) the bending of the uranyl subunit by comparing the spectrum of the bare uranyl in a linear and bent conformations; 2) the ligand-field of the chloride ligands in

Table 4: SO-TDDFT/CAM-B3LYP Vertical Transition Energies (in  $\text{cm}^{-1}$ ) and Oscillator Strengths in the  $\text{UO}_2\text{Cl}_2$ , and  $\text{UO}_2\text{Cl}_2(\text{phen})_2$  Molecules Computed at the PBE0-D3 Geometries.

$\text{UO}_2\text{Cl}_2$		
transitions	$\Delta E$	$f$
$\sigma_u(32\%) + \text{Cl}(62\%) \rightarrow \phi(87\%) + \delta(9\%)$	17 303	$1.95 \times 10^{-5}$
$\sigma_u(31\%) + \text{Cl}(63\%) \rightarrow \phi(93\%) + \delta(3\%)$	17 466	$8.70 \times 10^{-5}$
$\sigma_u(35\%) + \text{Cl}(59\%) \rightarrow \delta(77\%) + \phi(18\%)$	17 979	$7.95 \times 10^{-13}$
$\sigma_u(33\%) + \text{Cl}(58\%) \rightarrow \delta(77\%) + \phi(18\%)$	17 990	$8.12 \times 10^{-6}$
$\sigma_u(28\%) + \text{Cl}(63\%) \rightarrow \phi(62\%) + \delta(29\%)$	18 374	$1.40 \times 10^{-12}$
$\sigma_u(29\%) + \text{Cl}(64\%) \rightarrow \phi(71\%) + \delta(19\%)$	18 475	$8.11 \times 10^{-7}$
$\sigma_u(33\%) + \text{Cl}(59\%) \rightarrow \delta(69\%) + \phi(7\%)$	19 814	$9.42 \times 10^{-4}$
$\sigma_u(30\%) + \text{Cl}(63\%) \rightarrow \delta(77\%) + \delta(2\%)$	20 159	$1.26 \times 10^{-6}$
$\text{UO}_2\text{Cl}_2(\text{phen})_2$		
$\sigma_u + \text{Cl} \rightarrow \phi/\pi^*_{(\text{phen})_{ax}}(64\%) + \delta/\pi^*_{(\text{phen})_{ax}}(10\%)$	19 338	$1.02 \times 10^{-4}$
$\sigma_u + \text{Cl} \rightarrow \phi/\pi^*_{(\text{phen})_{ax}}(81\%) + \delta/\pi^*_{(\text{phen})_{ax}}(2\%)$	19 507	$3.49 \times 10^{-5}$
$\sigma_u + \text{Cl} \rightarrow \phi/\pi^*_{(\text{phen})_{ax}}(81\%) + \delta/\pi^*_{(\text{phen})_{ax}}(2\%)$	19 601	0.0
$\sigma_u + \text{Cl} \rightarrow \delta/\pi^*_{(\text{phen})_{ax}}$	19 656	$1.71 \times 10^{-7}$
$\sigma_u + \text{Cl} \rightarrow \phi/\pi^*_{(\text{phen})_{ax}}(75\%) + \delta/\pi^*_{(\text{phen})_{ax}}(5\%)$	20 516	0.0
$\sigma_u + \text{Cl} \rightarrow \phi/\pi^*_{(\text{phen})_{ax}}(75\%)$	20 666	$3.73 \times 10^{-5}$
$\sigma_u + \text{Cl} \rightarrow \delta/\pi^*_{(\text{phen})_{ax}}(52\%) + \phi/\pi^*_{(\text{phen})_{ax}}(9\%)$	21 515	$7.28 \times 10^{-4}$
$\sigma_u + \text{Cl} \rightarrow \delta/\pi^*_{(\text{phen})_{ax}}(56\%) + \delta/\pi^*_{(\text{phen})_{eq}}(6\%)$	21 983	$1.70 \times 10^{-6}$

$\text{UO}_2\text{Cl}_2$ , and that of the phenanthroline groups; and 3) the strength of spin-orbit coupling by comparing two-component (SO) and scalar relativistic (SR) results. The ten lowest TDDFT SO-excited states and their transitions, are listed in Table 3 and Table 4, while the corresponding SR values, as well as the TDDFT results, are reported in Supporting Information (Table S5, Table S6, Table S7). We note that a comparison of TDDFT and TDDFT/TDA (Tamm-Dancoff Approximation) results has been suggested in the literature<sup>73</sup> as a way to differentiate local and charge-transfer excitations – discrepancies between the results of the two calculations being the signature of charge-transfer excitations. We report differences up to  $600\text{ cm}^{-1}$  between TDDFT and TDDFT/TDA results for  $\text{UO}_2\text{Cl}_2$  (See Table S8), thus indicating that although the excited states involve both chloride 3p orbitals and the uranyl  $\sigma_u$ , the charge-transfer per say is not significant, and is well captured by the range-separated CAM-B3LYP functional.

Further evidence that contributions from charge-transfer should not play a significant role for the low-lying spectrum of uranyl-containing complexes with chloride ligands is found in the relatively small differences in excitation energies between calculations for the  $\text{UO}_2\text{Cl}_4^{2-}$  molecule and for the  $\text{UO}_2^{2+}$  ion embedded into the potential of the four chlorides in the equatorial plane,<sup>31</sup> since in the latter transitions to or from the chloride ligands are absent by construction. This embedding model can be considered as a rather flexible analogue to a ligand field treatment, based entirely on DFT calculations and in which not only electrostatic but electron correlation and orthogonalization effects are taken into account. We observe a fairly systematic red shift of about  $1000\text{ cm}^{-1}$ , for the lowest 12 excited states of the embedded  $\text{UO}_2^{2+}$  model. The differences in spacing between the different excited states are somewhat larger for the three low-lying excited states, reaching about  $600\text{ cm}^{-1}$ , but fall down to less than  $100\text{ cm}^{-1}$  for higher-lying states.

In  $\text{UO}_2\text{Cl}_2(\text{phen})_2$ , the  $\text{U}\equiv\text{O}$  bond distances are longer by almost  $0.1\text{ \AA}$  than those optimized for the bare uranyl ion in its electronic ground state,<sup>18</sup> and very close to those in the optimal geometry of the first-excited (luminescent) state.<sup>22</sup> The transition energies reported

in Table 3 are thus closer to emission energies for the bare uranyl species, and they cannot be directly compared to the values reported in the literature.<sup>18,22</sup>

In the bare uranyl unit (Table 3), the first seven excited states arise from excitations from the  $\sigma_u$  highest occupied molecular orbital (HOMO) into the nonbonding  $\delta$ ,  $\phi$  manifold, followed by transitions out of the  $\pi_u$  orbitals. Bending stabilizes the transitions to the  $\phi$  spinors by  $597\text{ cm}^{-1}$  at most, while the  $\delta$  spinors are stabilized by about  $435\text{ cm}^{-1}$ . However, bending the uranyl unit maintains the  $\sigma_u\phi$  character of the lowest luminescent state.

With the two coordinated chlorides, all transitions are shifted up by about  $3000\text{ cm}^{-1}$  as compared to those of the bent  $\text{UO}_2^{2+}$  (see Table 3 and Table 4); still the lowest excited states correspond to excitation to the  $\phi$  nonbonding orbital as in the bare uranyl unit. In  $\text{UO}_2\text{Cl}_2$ , the nature of accepting nonbonding orbitals in the first eight excited states resembles that of the bare bent uranyl cation, but doubly occupied 3p orbitals of the coordinated chlorines, that appear as the LUMO, contribute to the excitations up to about 60% and mix with contributions from the doubly occupied  $\sigma_u$  orbital that lies below the chloride 3p manifold. Note that because of limitations in the active space size, the preceding SO-CASPT2 calculations by Su *et al.*<sup>22</sup> did not include the chloride 3p orbitals, thus making it impossible to see any such contributions to the transitions.

The binding of the phenanthroline groups shifts all transition energies further up, so that these now start at  $19338\text{ cm}^{-1}$ , in line with the experimentally recorded spectrum. It is noteworthy that two lowest states with  $\phi$  character are only separated by about  $318\text{ cm}^{-1}$  from the next two states with  $\delta$  character. The molecular orbitals participating in the four lowest excited states are shown in Figure 2, revealing that the orbital out of which the electrons are excited from is centered on the  $\text{UO}_2\text{Cl}_2$  subunit involving a mixture of chloride 3p orbitals and the uranyl  $\sigma_u$ . For the lowest two excited states, the accepting orbital has a uranium  $5f_\phi$  character. In the third and fourth states, the accepting spinor has a dominant  $5f_\delta$  character. Moving up in energy, a spinor with  $\pi^*$  of the axial phenanthroline group mixes in. In that sense, the low-lying excitations remain strongly localized on the  $\text{UO}_2\text{Cl}_2$  subunit,

with a character that resembles  $[\sigma_u + \text{Cl}(3p) \rightarrow \text{U}(f)]$  but there are now non-negligible contributions from spinors/orbitals located over the axial phenanthroline group.

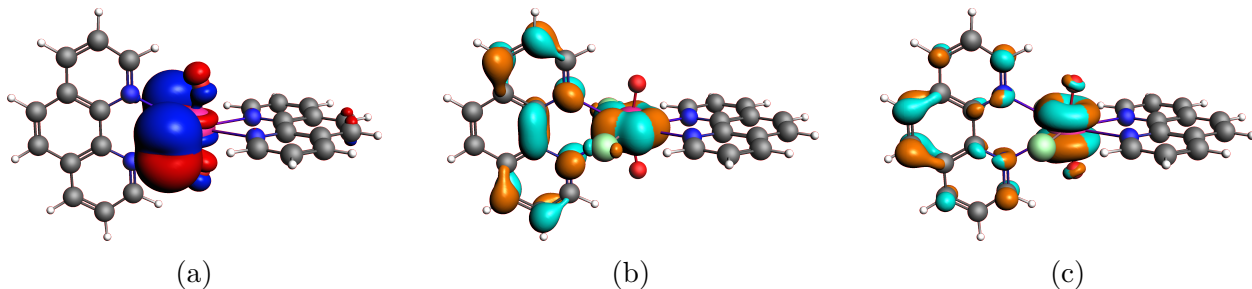


Figure 2: Molecular spinors: (a) occupied orbital from which the electron is excited; (b) empty orbital accepting the electron in the first three excited states; c) empty orbital accepting the electron in the fourth excited state. Isosurface values are  $\pm 0.03$  au.

## Ligand-Field Effects and Spin-Orbit Coupling

As discussed by Su *et al.*<sup>22</sup> the nature of the luminescent state is determined by the competition between SO-coupling, which stabilizes more the  $\phi$  orbitals than the  $\delta$  ones, and the ligand-field splitting, which may destabilize the  $\phi$  and  $\delta$  orbitals depending on the ligands. It is possible to quantify these two effects: the ligand-field splitting can be measured by the difference of the SR transition energies for states with  $\phi/\delta$  characters in a molecular complex with respect to the corresponding ones in the bare uranyl species; the spin-orbit stabilization is simply computed as the difference between the lowest state with a dominant  $\phi/\delta$  and its SR triplet counterpart.

As revealed by the values of Table 5, in the bare linear and bent uranyl the  $\phi$  SR states lie about 1433 and 1743  $\text{cm}^{-1}$  below the  $\delta$  states, in the linear and bent moieties, respectively. As its SO stabilization is larger (about  $-3580$  and  $-3483$   $\text{cm}^{-1}$ ) than that of the  $\delta$  state (about  $-2153$  and  $-2103$   $\text{cm}^{-1}$ ), the lowest SO excited state has a  $\phi x'$  character. In  $\text{UO}_2\text{Cl}_4^{2-}$ , the state ordering is different, as the four chlorides destabilize the  $\phi$  SR states far more, 7403  $\text{cm}^{-1}$ , than the  $\delta$  states, 2875  $\text{cm}^{-1}$ . This strong destabilization of the  $\phi$  SR states is not compensated by the larger SO energetic stabilization. As a result, the first excited state

Table 5: Energy Gaps ( $E_{\text{SR}}(\delta) - E_{\text{SR}}(\phi)$ ) between the Triplet SR states Dominated by Excitations into the  $\delta$  and  $\phi$  Orbitals (Positive Values Mean That the  $\delta$  State is above the  $\phi$  State); Ligand-Field Splittings of the SR States Dominated by Excitations into the  $\delta$  and  $\phi$  Orbitals ( $E_{\text{LF}}(\delta/\phi)$ ); and Spin-Orbit Stabilizations of the SR States Dominated by Excitations into the  $\delta$  and  $\phi$  Orbitals ( $\Delta E_{\text{SO}}(\delta/\phi)$ ) (All Values in  $\text{cm}^{-1}$  and Computed in the Gas Phase)

Compound	$E_{\text{SR}}(\delta) - E_{\text{SR}}(\phi)$	$\Delta E_{\text{LF}}(\phi)$	$\Delta E_{\text{LF}}(\delta)$	$\Delta E_{\text{SO}}(\phi)$	$\Delta E_{\text{SO}}(\delta)$
linear $\text{UO}_2^{2+}$	1433			-3580	-2103
bent $\text{UO}_2^{2+}$	1743			-3483	-2153
$[\text{UO}_2\text{Cl}_4]^{2-}$	-3095	7403	2875	-5199	-2432
$\text{UO}_2\text{Cl}_2$	-1053	3547	1060	-3920	-2190
$\text{UO}_2\text{Cl}_2(\text{phen})_2$	-1657	5959	2869	-4297	-2377

has a  $\delta$  character and involves excitations out of both the  $\sigma_u$  uranyl orbital and the chloride 3p orbitals. In  $\text{UO}_2\text{Cl}_2$  and  $\text{UO}_2\text{Cl}_2(\text{phen})_2$ , the ligand-field effect is not as strong as in the tetrachlorouranyl complex; the chloride and phenanthroline groups destabilize the  $\phi$  SR states far more than the  $\delta$  states (3547 versus 1060  $\text{cm}^{-1}$  in  $\text{UO}_2\text{Cl}_2$ , and 5959  $\text{cm}^{-1}$  versus 2869  $\text{cm}^{-1}$  in  $\text{UO}_2\text{Cl}_2(\text{phen})_2$ ). The SO stabilization effects are almost the same as in the bare unit, that is about 1920  $\text{cm}^{-1}$  larger for the  $\phi$  states than the  $\delta$  states, thus placing the SO states with a  $\delta$  character a few  $\text{cm}^{-1}$  higher than the  $\phi$  ones.

The excellent agreement between the computed and experimental vertical absorption energies for  $[\text{UO}_2\text{Cl}_4]^{2-}$  (see Table 3) demonstrates that the energy spacing within the excited state manifold is accurately captured by CAM-B3LYP. Taken together with the results for the embedded model<sup>31</sup> for  $\text{UO}_2^{2+}$  mentioned above, these results make us confident about the ability of CAM-B3LYP to accurately capture the effects ligand-field and SO splittings on the low-lying valence states of uranyl complexes.

## Emission Spectra of $\text{UO}_2\text{Cl}_2$ and $\text{UO}_2\text{Cl}_2(\text{phen})_2$

Luminescence spectroscopy is one of the experimental techniques that can probe chemical interactions of U(VI) with the equatorial ligands of a complex. Uranium (VI) complexes display specific luminescence features with characteristic band shapes that mostly depend

on the chemical composition of the closest environment of uranyl unit. The luminescence spectrum of  $\text{UO}_2\text{Cl}_2$  has been recorded previously at 4 K in Ar matrix conditions and reported by Jin *et al.*<sup>64</sup>(Figure 3(a)). In our study the  $\text{UO}_2\text{Cl}_2(\text{phen})_2$  luminescence spectra are obtained at 80 and 298 K as it is shown on Figure 3(b). Both compounds exhibit the same type of progression with the difference in spectral lines resolution that mostly depends on the contributions from the thermally active bands induced by the temperature effects.<sup>74</sup>

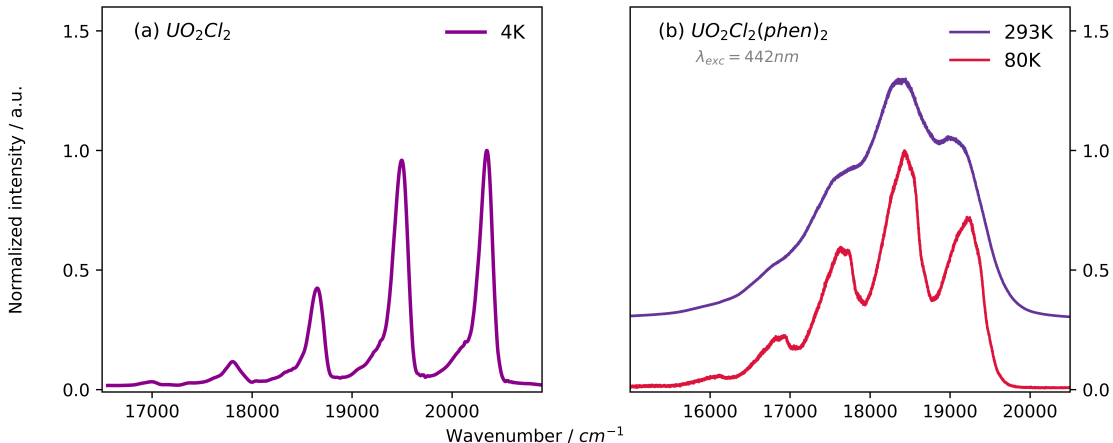


Figure 3: Normalized experimental luminescence spectra of (a)  $\text{UO}_2\text{Cl}_2$  at 4 K and (b)  $\text{UO}_2\text{Cl}_2(\text{phen})_2$  spectra recorded at 80 and 293 K after 442 nm excitation. The spectrum in (a) was reconstructed from ref 64. Copyright 2009 American Chemical Society.

Experimentally, the luminescence of uranium(VI) complexes originates at  $20\,343\text{ cm}^{-1}$  for  $\text{UO}_2\text{Cl}_2$  and  $19\,135\text{ cm}^{-1}$  in the case of  $\text{UO}_2\text{Cl}_2(\text{phen})_2$ . Such a shift is observed because of the changes in the overall basicity of the complex. At a low-temperature Ar as the Lewis base can bind to uranium,<sup>22</sup> but the presence of a lone pair of electrons of nitrogen of phenanthroline ligands makes it more basic as compared to Ar, which causes a luminescence origin shift to lower wavenumbers. For instance, in  $\text{UO}_2\text{Cl}_4^{2-}$  the nature of equatorial ligands is the same as in  $\text{UO}_2\text{Cl}_2$  and its experimental luminescence origin corresponds to  $20\,096\text{ cm}^{-1}$ <sup>75</sup> and matches well with the value obtained for  $\text{UO}_2\text{Cl}_2$ . In general, the luminescence spectrum of uranium(VI) complexes results from the electronic transitions from the low-lying excited states to the ground state coupled to vibronic progression. Whereas the overall nature of

uranium(VI) luminescence is still a topic for discussion since it might consist of radiative and nonradiative processes, the direct comparison between theoretical and experimental electronic transition energies is misleading. Yet here we could discuss the nature of the radiative part of  $\text{UO}_2\text{Cl}_2$  and  $\text{UO}_2\text{Cl}_2(\text{phen})_2$  luminescence deduced from theoretical calculations of emission energies and vibronic progressions.

Theoretical vertical emission energies were obtained from the  $\sigma_u\phi$  lowest excited state structures of  $\text{UO}_2\text{Cl}_2$  and  $\text{UO}_2\text{Cl}_2(\text{phen})_2$  complexes and are reported in Table 6. While for the large  $\text{UO}_2\text{Cl}_2(\text{phen})_2$  complex, the computed and experimental data, 18 464 and 19 135  $\text{cm}^{-1}$ , respectively, closely match, for  $\text{UO}_2\text{Cl}_2$ , the computed emission energy comes out 3814  $\text{cm}^{-1}$  too low compared to experiment. Note that Su *et al.*<sup>22</sup> reported emission energies of 18 509  $\text{cm}^{-1}$  and 18 797  $\text{cm}^{-1}$  at the SO-CASPT2 and SO-CCSD(T) levels for  $\text{UO}_2\text{Cl}_2$ , respectively, also too low as compared to the experimental value of 20 323  $\text{cm}^{-1}$ . To check whether this discrepancy arises from the argon matrix, we also performed TDDFT/CAM-B3LYP calculations on  $\text{UO}_2\text{Cl}_2\text{Ar}_2$  used as a model for  $\text{UO}_2\text{Cl}_2$  immersed in an argon matrix. Their SO-CCSD(T) calculations (Table 8 of ref 22) and our TDDFT/CAM-B3LYP ones (see Table S8) both show that argon insignificantly modifies the transition energy. Therefore, we suspect that this inaccuracy for  $\text{UO}_2\text{Cl}_2$  might be correlated with the underestimation observed for the bare uranyl molecule discussed earlier and requires a detailed investigation on its own.

For deep analysis, the vibronic progressions of the  $\text{UO}_2\text{Cl}_2$  and  $\text{UO}_2\text{Cl}_2(\text{phen})_2$  complexes out of the first excited state to the ground state were computed using their structures, as well as associated harmonic frequency spectra together with Hessian matrices. The main vibronic progression of uranium(VI) compounds is usually formed by the major contribution from the ground state symmetric stretching mode of the uranyl unit coupling with minor contributions from other vibrational modes that depend on the complex structure and composition mainly. Here we are aiming at providing the assignment of visible spectral bands that were observed in the emission spectra. In Figure 4, red curves correspond to experimental spectra of

Table 6: SO-TDDFT Emission Energies (in  $\text{cm}^{-1}$ ) and Oscillator Strengths of  $\text{UO}_2\text{Cl}_2$  and  $\text{UO}_2\text{Cl}_2(\text{phen})_2$  Computed at the PBE0-D3 Geometries in the Gas Phase.

$\text{UO}_2\text{Cl}_2$		
transitions	$\Delta E$	$f$
$\sigma_u(37\%) + \text{Cl}(45\%) \rightarrow \phi$	16 529	$1.55 \times 10^{-5}$
$\sigma_u(37\%) + \text{Cl}(45\%) \rightarrow \phi$	16 678	$7.84 \times 10^{-5}$
$\sigma_u(37\%) + \text{Cl}(45\%) \rightarrow \delta(50\%) + \phi(40\%)$	17 301	$2.00 \times 10^{-12}$
$\sigma_u(37\%) + \text{Cl}(45\%) \rightarrow \delta(56\%) + \phi(33\%)$	17 330	$4.61 \times 10^{-6}$
$\sigma_u(37\%) + \text{Cl}(45\%) \rightarrow \phi(49\%) + \delta(41\%)$	17 659	$1.32 \times 10^{-11}$
$\sigma_u(37\%) + \text{Cl}(45\%) \rightarrow \phi(54\%) + \delta(35\%)$	17 733	$1.64 \times 10^{-6}$
$\sigma_u(37\%) + \text{Cl}(45\%) \rightarrow \delta(82\%) + \phi(6\%)$	19 147	$9.29 \times 10^{-4}$
$\sigma_u(37\%) + \text{Cl}(45\%) \rightarrow \delta$	19 529	$3.79 \times 10^{-6}$
$\text{UO}_2\text{Cl}_2(\text{phen})_2$		
transitions	$\Delta E$	$f$
$\sigma_u + \text{Cl} \rightarrow \phi(57\%) + \delta/\pi_{(\text{phen})_{ax}}^*(14\%)$	18 464	$1.23 \times 10^{-4}$
$\sigma_u + \text{Cl} \rightarrow \phi(62\%) + \delta/\pi_{(\text{phen})_{eq}}^*(20\%)$	18 629	$3.33 \times 10^{-5}$
$\sigma_u + \text{Cl} \rightarrow \delta/\pi_{(\text{phen})_{ax}}^*(58\%) + \phi(3\%)$	18 919	$7.71 \times 10^{-9}$
$\sigma_u + \text{Cl} \rightarrow \delta/\pi_{(\text{phen})_{ax}}^*(58\%)$	18 982	$8.00 \times 10^{-7}$
$\sigma_u + \text{Cl} \rightarrow \phi(79\%) + \delta/\pi_{(\text{phen})_{eq}}^*(27\%)$	19 676	$1.07 \times 10^{-9}$
$\sigma_u + \text{Cl} \rightarrow \phi(62\%) + \delta/\pi_{(\text{phen})_{eq}}^*(15\%)$	19 766	$3.94 \times 10^{-5}$
$\sigma_u + \text{Cl} \rightarrow \delta/\pi_{(\text{phen})_{eq}}^*(30\%) + \delta/\pi_{(\text{phen})_{eq}}^*(16\%)$	20 738	$8.62 \times 10^{-4}$
$\sigma_u + \text{Cl} \rightarrow \delta/\pi_{(\text{phen})_{ax}}^*$	21 434	$1.63 \times 10^{-4}$

$\text{UO}_2\text{Cl}_2$  in Ar matrix at 4 K (top panel),  $\text{Cs}_2\text{UO}_2\text{Cl}_4$  crystal at 80 K (middle panel) and  $\text{UO}_2\text{Cl}_2(\text{phen})_2$  at 80 K (bottom panel) while black vertical lines are corresponding theoretical vibronic progressions. For illustration purposes and clarity of comparison, both types of spectra were normalized by the maximum intensity value and theoretical ones were shifted to match the experimental luminescence origin. Figure 4 highlights the good agreement between the experimental and theoretical spectra since the band spacings of the computed vertical lines match nicely the experimental envelope.

The complete assignment of all obtained bands is provided in Table S10 and Table S11. Here we discuss only significant differences between  $\text{UO}_2\text{Cl}_2$ ,  $\text{UO}_2\text{Cl}_4^{2-}$  and  $\text{UO}_2\text{Cl}_2(\text{phen})_2$  vibronic contributions. The first observed transition for all three compounds is computed to be  $0'(0)\rightarrow 1(0)$  and corresponds to a 0 vibrational transition from the excited state to the ground state. The structure and symmetry of ligands in  $\text{UO}_2\text{Cl}_2$  and  $\text{UO}_2\text{Cl}_2(\text{phen})_2$  complexes enable the uranyl bending mode to become vibronically excited and appear on the spectrum in the range of 219 to 281  $\text{cm}^{-1}$ . Note that it is not the case for the  $\text{UO}_2\text{Cl}_4^{2-}$  complex because in this energy region the Cl-U-Cl symmetric stretching mode contribution is observed. The analysis of other computed bands showed no other significant contributions than the uranyl symmetric stretching mode, which means that the coupling scheme remains the same for all uranium(VI) complexes discussed in this study. Here the ground state symmetric stretching mode is computed to be placed at 949, 894 and 895  $\text{cm}^{-1}$  after the  $0'(0)\rightarrow 1(0)$  transition for  $\text{UO}_2\text{Cl}_2$ ,  $\text{UO}_2\text{Cl}_4^{2-}$  and  $\text{UO}_2\text{Cl}_2(\text{phen})_2$  respectively, which is slightly overestimated compared to the averaged experimental band spacing of 840, 817 and 794  $\text{cm}^{-1}$ , respectively. Since theoretical band spacing is somewhat red-shifted one should note that anharmonicity corrections are not accounted for causing even bigger band shifts.

It is worth mentioning the broadening of the experimental spectra. Despite the fact that the spectra were obtained at different low temperatures (4 and 80 K), as mentioned earlier, thermally active transitions do occur, but have been reduced to a minimum as much as possible. Their extent cannot be predicted, and thus, we eliminate direct comparison of  $\text{UO}_2\text{Cl}_2$

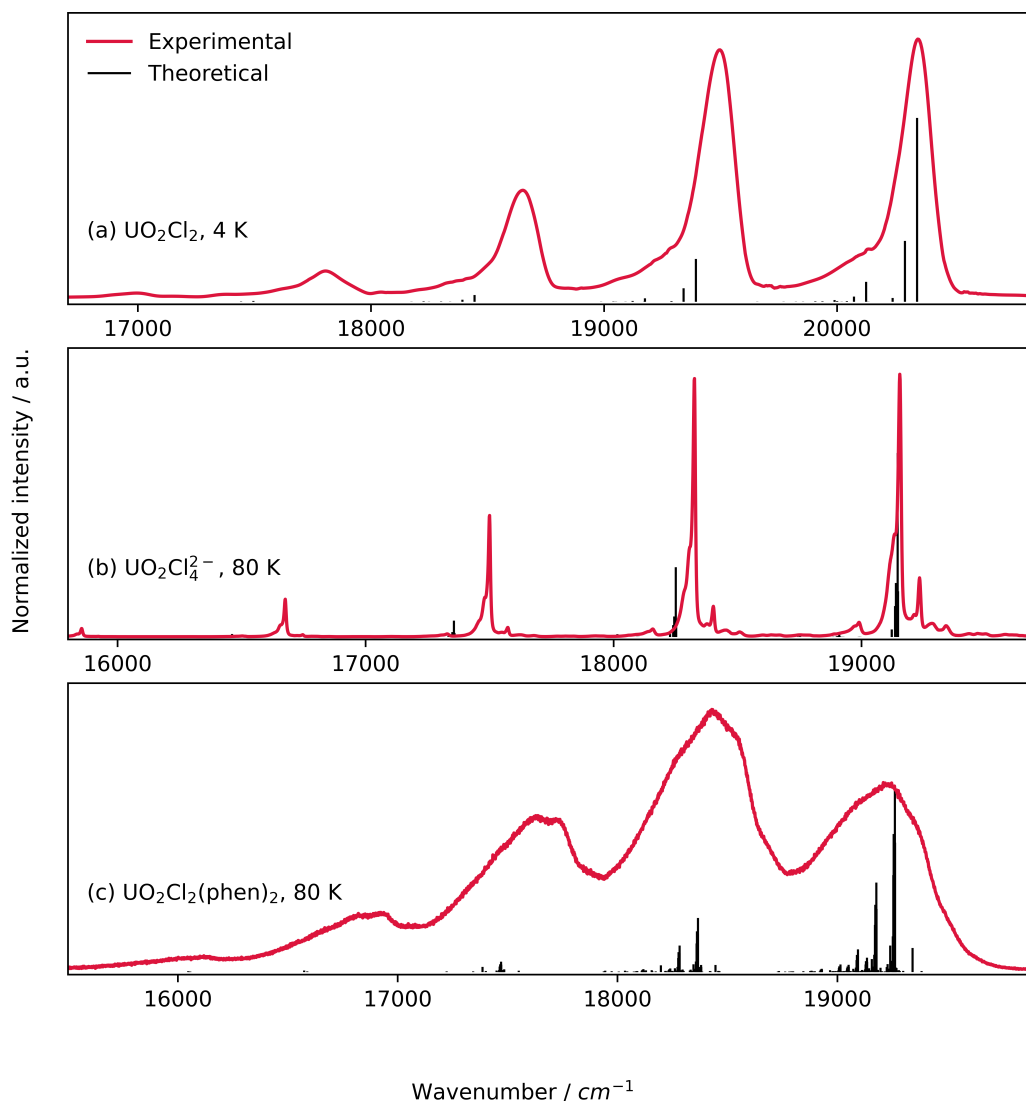


Figure 4: Comparison of theoretical and experimental luminescence spectra of (a)  $UO_2Cl_2$ , (b)  $Cs_2UO_2Cl_4$ , and (c)  $UO_2Cl_2(phen)_2$  complexes. The origins of the theoretical spectra are shifted by (a) 3814, (b) 172, and (c) 671  $cm^{-1}$  to match the experimental peaks. The spectrum in (a) was reconstructed from ref 64. Copyright 2009 American Chemical Society.

broadening with  $\text{UO}_2\text{Cl}_4^{2-}$  and  $\text{UO}_2\text{Cl}_2(\text{phen})_2$  ones. Nevertheless, we observe that in the spectra obtained at a temperature of 80 K, the width of the bands is not consistent. From the point of view of radioactive processes, if we refer to Figure 4 as well as to the assignment provided in Table S10, it can be seen visually that the number of bands in the 50 to 400  $\text{cm}^{-1}$  region after the  $0'(0) \rightarrow 1(0)$  transition is much larger in the case of  $\text{UO}_2\text{Cl}_2(\text{phen})_2$  than in  $\text{UO}_2\text{Cl}_4^{2-}$ . This phenomenon could be explained by the uranyl bending mode coupling with the ligand motions that are induced by the uranyl bent structure.

## Conclusions

We have synthesized the bent  $\text{UO}_2\text{Cl}_2(\text{phen})_2$ , confirming the structure reported by Schöne *et al.*<sup>10</sup>. The QC calculations provide a rationale for the geometry of  $\text{UO}_2\text{Cl}_2(\text{phen})_2$ . They demonstrate that the axial phenanthroline group largely contributes to making the bent actinyl structure energetically stable. QTAIM and NBO analysis, however, indicate the the nature of the  $\text{U}-\text{O}_{\text{yl}}$  bond does not change upon bending, a fact that could be further investigated via quantum entanglement methods, as done by Leszczyk *et al.*<sup>76</sup>. In this study, we investigated the influence of the bending of the uranyl moiety and of the coordinated chloride and phenanthroline ligands with the help of spin-orbit coupled TDDFT calculations to determine the nature of the low-lying excited states of bare uranyl complexes versus those of uranyl tetrachloride, uranyl dichloride and  $\text{UO}_2\text{Cl}_2(\text{phen})$ . While in uranyl tetrachloride, the lowest electronic state causing luminescent emission has a predominant  $5f_\delta$  character, the emitting state of all three complexes uranyl,  $\text{UO}_2\text{Cl}_2$  and  $\text{UO}_2\text{Cl}_2(\text{phen})_2$  has a  $5f_\phi$  character. The two chloride and phenanthroline ligands cause a larger destabilization of the  $\phi$  states than of the  $\delta$  states but at the same time a smaller SO splitting of the former than the latter. As a result, the energy gap between the lowest  $\phi$  and  $\delta$  SO states is as small as about 300  $\text{cm}^{-1}$ , as opposed to 3000  $\text{cm}^{-1}$  in bare uranyl complexes.

Using SO-TDDFT/CAM-B3LYP calculations coupled with vibronic coupling simulations

allows computation of the vibrational progressions of the emission spectra, for a direct comparison with the experimental spectra available for  $\text{UO}_2\text{Cl}_2$  (though in an argon matrix) and  $\text{Cs}_2\text{UO}_2\text{Cl}_4$ , and to the luminescence spectrum of  $\text{UO}_2\text{Cl}_2(\text{phen})_2$  measured for the first time at 80 K. Despite the need of shifting the origin of the computed spectrum with respect to the experimental one, the spacing between the computed vibronic bands matches the experimental spectra envelopes. The presence of a bent uranyl moiety in  $\text{UO}_2\text{Cl}_2$  and  $\text{UO}_2\text{Cl}_2(\text{phen})_2$  complexes triggers vibronic excitations of the uranyl bending motion predominantly in the range of 219 to 281  $\text{cm}^{-1}$ , broadening significantly the spectrum around the dominant progression that corresponds to the uranyl symmetric stretching mode. This broadening is a signature of the bending of uranyl, but it might also arise from motions of equatorial ligands, such as bromide in  $\text{UO}_2\text{Br}_4^{2-}$ . In practice, QC simulations have reached a reliable level of accuracy making them a first-choice methodology to discuss and assign emission spectra of uranyl complexes.

## Acknowledgements

ASPG and VV acknowledge support from PIA ANR project CaPPA (ANR-11-LABX-0005-01), the Franco-German project ComprIXS (Agence nationale de la recherche ANR-19-CE29-0019, Deutsche Forschungsgemeinschaft JA 2329/6-1), I-SITE ULNE projects OVERSEE and MESONM International Associated Laboratory (LAI) (ANR-16-IDEX-0004), the French Ministry of Higher Education and Research, region Hauts de France council and European Regional Development Fund (ERDF) project CPER CLIMIBIO, WaveTech and the French national supercomputing facilities (grants DARI A0130801859, A0110801859). HO, ASPG and VV also acknowledge funding by the ANR project ANR-21-CE29-0027. Experimental work was conducted at ANL, operated by UChicago Argonne LLC for the United States Department of Energy (U.S. DOE), and supported by the U.S. DOE Office of Science, Office of Basic Energy Sciences, Chemical Sciences Geological and Biosciences

Division, Heavy Element Chemistry program under Contract DE-AC02-06CH11357. The authors acknowledge Sergey Telnov for his artistic contribution to graphical art.

## Associated content

The data (input/output) corresponding to the QC calculations of this paper are available at the Zenodo repository under DOI: <http://doi.org/10.5281/zenodo.7702590>.

The Supporting Information is available free of charge on the ACS Publications website at DOI: XXX. Justification for performing the calculations in the gas-phase. Table summarizing the QTAIM and NBO data (Table S4), scalar relativistic transition energies (Table S5, Table S6, Table S7), comparison of TDDFT and TDA transition energies for  $\text{UO}_2\text{Cl}_2$  and TDDFT energies of  $\text{UO}_2\text{Cl}_2\text{Ar}_2$  (Table S8), TDDFT transition energies of  $\text{UO}_2\text{Cl}_2(\text{phen})_2$  computed at with the SR-ZORA Hamiltonian in the gas phase and the COSMO water solvent (Table S9),  $\text{UO}_2\text{Cl}_2$ ,  $\text{UO}_2\text{Cl}_4^{2-}$  and  $\text{UO}_2\text{Cl}_2(\text{phen})_2$  luminescence spectra assignment computed in the gas-phase at 4K (Table S10, Table S11). The FT-IR and Raman spectra of  $\text{UO}_2\text{Cl}_2(\text{phen})_2$  under  $^{18}\text{O}$  exchange (Figure S1, Figure S2).

## Note

A preprint version of this work was deposited at ChemRxiv.<sup>77</sup>

## References

- (1) Grenthe, I.; Drożdżyński, J.; Fujino, T.; Buck, E. C.; Albrecht-Schmitt, T. E.; Wolf, S. F. In *The Chemistry of the Actinide and Transactinide Elements*, 3rd ed.; Morss, L. R., Edelstein, N. M., Fuger, J., Eds.; Springer: Dordrecht, The Netherlands, 2006; Chapter 5, pp 253–698, DOI: 10.1007/1-4020-3598-5\_5.
- (2) Hayton, T. W. Understanding the origins of  $O_{yl}-U-O_{yl}$  bending in the uranyl ( $UO_2^{2+}$ ) ion. *Dalton Trans.* **2018**, 47, 1003–1009, DOI: 10.1039/c7dt04123c.
- (3) Dylla, K. G. Bonding and bending in the actinyls. *Mol. Phys.* **1999**, 96, 511, DOI: 10.1080/00268979909482988.
- (4) Sunaga, A.; Tabata, C.; Yamamura, T. Linearity and Chemical Bond of  $UO_2^{2+}$  Revisited: A Comparison Study with  $UN_2$  and  $UE_2^{2+}$  (E = S, Se, and Te) Based on Relativistic Calculations. *J. Phys. Chem. A* **2022**, 126, 8606–8617, DOI: 10.1021/acs.jpca.2c05216.
- (5) Hratchian, H. P.; Sonnenberg, J. L.; Hay, P. J.; Martin, R. L.; Bursten, B. E.; Schlegel, H. B. Theoretical investigation of uranyl dihydroxide: oxo ligand exchange, water catalysis, and vibrational spectra. *J. Phys. Chem. A* **2005**, 109, 8579–8586, DOI: 10.1021/jp052616m.
- (6) Schreckenbach, G.; Hay, P. J.; Martin, R. L. Theoretical study of stable trans and cis isomers in  $[UO_2(OH)_4]^{2-}$  using relativistic density functional theory. *Inorg. Chem.* **1998**, 37, 4442, DOI: 10.1021/ic980057a.
- (7) Schreckenbach, G.; Hay, P. J.; Martin, R. L. Density functional calculations on actinide compounds: survey of recent progress and application to  $[UO_2X_2]^{2-}$  (X=F, Cl, OH) and  $AnF_6$  (An = U, Np, Pu). *J. Comp. Chem.* **1999**, 20, 70–90, DOI: 10.1002/(SICI)1096-987X(19990115)20:1<70::AID-JCC9>3.0.CO;2-F.

- (8) Vallet, V.; Wahlgren, U.; Grenthe, I. Probing the Nature of Chemical Bonding in Uranyl(VI) Complexes with Quantum Chemical Methods. *J. Phys. Chem. A* **2012**, *116*, 12373–12380, DOI: 10.1021/jp3091123.
- (9) Pietro, P. D.; Kerridge, A. U–O<sub>yl</sub> Stretching Vibrations as a Quantitative Measure of the Equatorial Bond Covalency in Uranyl Complexes: A Quantum-Chemical Investigation. *Inorg. Chem.* **2016**, *55*, 573–583, DOI: 10.1021/acs.inorgchem.5b01219.
- (10) Schöne, S.; Radoske, T.; März, J.; Stumpf, T.; Patzschke, M.; Ikeda-Ohno, A. [UO<sub>2</sub>Cl<sub>2</sub>(phen)<sub>2</sub>], a Simple Uranium(VI) Compound with a Significantly Bent Uranyl Unit (phen = 1,10-phenanthroline). *Chem. Eur. J.* **2017**, *23*, 13574–13578, DOI: 10.1002/chem.201703009.
- (11) Langer, E. M.; Kegler, P.; Kowalski, P. M.; Wang, S.; Alekseev, E. V. Achieving and Stabilizing Uranyl Bending via Physical Pressure. *Inorg. Chem.* **2021**, *60*, 8419–8422, DOI: 10.1021/acs.inorgchem.1c00644.
- (12) Carter, K. P.; Kalaj, M.; Cahill, C. L. Probing the Influence of N-Donor Capping Ligands on Supramolecular Assembly in Molecular Uranyl Materials. *Eur. J. Inorg. Chem.* **2016**, *2016*, 126–137, DOI: 10.1002/ejic.201501118.
- (13) Carter, K. P.; Kalaj, M.; Kerridge, A.; Ridenour, J. A.; Cahill, C. L. How to Bend the Uranyl Cation via Crystal Engineering. *Inorg. Chem.* **2018**, *57*, 2714–2723, DOI: 10.1021/acs.inorgchem.7b03080, PMID: 29436823.
- (14) Zhang, Z.; Pitzer, R. M. Application of relativistic quantum chemistry to the electronic energy levels of the uranyl ion. *J. Phys. Chem. A* **1999**, *103*, 6880–6886, DOI: 10.1021/jp991867q.
- (15) Denning, R. G. *Complexes, Clusters and Crystal Chemistry*; Springer, 1992; Vol. 79; pp 215–276, DOI: 10.1007/BFb0036502.

- (16) Denning, R. G. Electronic structure and bonding in actinyl ions and their analogs. *J. Phys. Chem. A* **2007**, *111*, 4125–4143, DOI: 10.1021/jp071061n.
- (17) Matsika, S.; Pitzer, R. M. Actinyl ions in  $\text{Cs}_2\text{UO}_2\text{Cl}_4$ . *J. Phys. Chem. A* **2001**, *105*, 637–645, DOI: 10.1021/jp003032h.
- (18) Réal, F.; Gomes, A. S. P.; Visscher, L.; Vallet, V.; Eliav, E. Benchmarking Electronic Structure Calculations on the Bare  $\text{UO}_2^{2+}$  ion: How Different are Single and Multireference Electron Correlation Methods? *J. Phys. Chem. A* **2009**, *113*, 12504–12511, DOI: 10.1021/jp903758c.
- (19) Pierloot, K.; van Besien, E. Electronic structure and spectrum of  $\text{UO}_2^{2+}$  and  $\text{UO}_2\text{Cl}_4^{2-}$ . *J. Chem. Phys.* **2005**, *123*, 204309, DOI: 10.1063/1.2121608.
- (20) Réal, F.; Vallet, V.; Marian, C.; Wahlgren, U. Theoretical investigation of the energies and geometries of photo-excited uranyl(VI) ion: a comparison between wavefunction theory and density functional theory. *J. Chem. Phys.* **2007**, *127*, 214302, DOI: 10.1063/1.2814157.
- (21) Tecmer, P.; Gomes, A. S. P.; Ekström, U.; Visscher, L. Electronic Spectroscopy of  $\text{UO}_2^{2+}$ , NUN and  $\text{NUO}^+$ . *Phys. Chem. Chem. Phys.* **2011**, *13*, 6249–6259, DOI: 10.1039/c0cp02534h.
- (22) Su, J.; Wang, Y.-L.; Wei, F.; Schwarz, W. H. E.; Li, J. Theoretical Study of the Luminescent States and Electronic Spectra of  $\text{UO}_2\text{Cl}_2$  in an Argon Matrix. *J. Chem. Theory Comput.* **2011**, *7*, 3293–3303, DOI: 10.1021/ct200419x.
- (23) Shen, G.; Guo, M.; Wang, Z.; Wang, F. Effects of ligands on excitation energies of  $[\text{UO}_2\text{X}_4]^{2-}$  and  $\text{UO}_2\text{X}_2$  ( $\text{X} = \text{F}, \text{Cl}$ ) with the equation-of-motion coupled-cluster theory. *Int. J. Quantum Chem.* **2022**, *122*, e26981, DOI: 10.1002/qua.26981.

- (24) Kaltsoyannis, N.; Hay, P. J.; Li, J.; Blaudeau, J.-P.; Bursten, B. E. In *The Chemistry of the Actinide and Transactinide Elements*, 4th ed.; Morss, L. R., Edelstein, N. M., Fuger, J., Eds.; Springer: Dordrecht, The Netherlands, 2010; Vol. 3; Chapter 17, pp 1893–2012, DOI: 10.1007/978-94-007-0211-0\_17.
- (25) Gomes, A. S. P.; Réal, F.; Schimmelpfennig, B.; Wahlgren, U.; Vallet, V. In *Computational Methods in Lanthanide and Actinide Chemistry*; Dolg, M., Ed.; John Wiley & Sons Ltd, 2015; Chapter 11, pp 269–298, DOI: 10.1002/9781118688304.ch11.
- (26) Leszczyk, A.; Tecmer, P.; Boguslawski, K. In *Transition Metals in Coordination Environments. Challenges and Advances in Computational Chemistry and Physics*; Broclawik E., R. M., Borowski T., Ed.; Springer, 2019; Vol. 29; pp 121–160, DOI: 10.1007/978-3-030-11714-6\_5.
- (27) Réal, F.; Vallet, V.; Wahlgren, U.; Grenthe, I. *Ab initio* study of the mechanism for photoinduced yl-oxygen exchange in uranyl(VI) in acidic aqueous solution. *J. Am. Chem. Soc.* **2008**, *130*, 11742–11751, DOI: 10.1021/ja8026407.
- (28) Su, J.; Wang, Z.; Pan, D.; Li, J. Excited States and Luminescent Properties of  $\text{UO}_2\text{F}_2$  and Its Solvated Complexes in Aqueous Solution. *Inorg. Chem.* **2014**, *53*, 7340–7350, DOI: 10.1021/ic5006852.
- (29) van Besien, E.; Pierloot, K.; Görrler-Walrand Electronic spectra of uranyl chloride complexes in acetone: a CASSCF/CASPT2 investigation. *Phys. Chem. Chem. Phys.* **2006**, *8*, 4311–4319, DOI: 10.1039/b607026d.
- (30) Pierloot, K.; van Besien, E.; van Lenthe, E.; Baerends, E. J. Electronic structure and spectrum of  $\text{UO}_2^{2+}$  and  $\text{UO}_2\text{Cl}_4^{2-}$  calculated with time-dependent density functional theory. *J. Chem. Phys.* **2007**, *126*, 194311, DOI: 10.1063/1.2735297.
- (31) Gomes, A. S. P.; Jacob, C. R.; Réal, F.; Visscher, L.; Vallet, V. Towards systematically improvable models for actinides in condensed phase: the electronic spectrum of uranyl

in  $\text{Cs}_2\text{UO}_2\text{Cl}_4$  as a test case. *Phys. Chem. Chem. Phys.* **2013**, *15*, 15153–15162, DOI: 10.1039/C3CP52090K.

- (32) Frisch, M. J.; Trucks, G. W.; Schlegel, H. B.; Scuseria, G. E.; Robb, M. A.; Cheeseman, J. R.; Scalmani, G.; Barone, V.; Petersson, G. A.; Nakatsuji, H.; Li, X.; Caricato, M.; Marenich, A. V.; Bloino, J.; Janesko, B. G.; Gomperts, R.; Menucci, B.; Hratchian, H. P.; Ortiz, J. V.; Izmaylov, A. F.; Sonnenberg, J. L.; Williams-Young, D.; Ding, F.; Lipparini, F.; Egidi, F.; Goings, J.; Peng, B.; Petrone, A.; Henderson, T.; Ranasinghe, D.; Zakrzewski, V. G.; Gao, J.; Rega, N.; Zheng, G.; Liang, W.; Hada, M.; Ehara, M.; Toyota, K.; Fukuda, R.; Hasegawa, J.; Ishida, M.; Nakajima, T.; Honda, Y.; Kitao, O.; Nakai, H.; Vreven, T.; Throssell, K.; Montgomery, J. A., Jr.; Peralta, J. E.; Ogliaro, F.; Bearpark, M. J.; Heyd, J. J.; Brothers, E. N.; Kudin, K. N.; Staroverov, V. N.; Keith, T. A.; Kobayashi, R.; Normand, J.; Raghavachari, K.; Rendell, A. P.; Burant, J. C.; Iyengar, S. S.; Tomasi, J.; Cossi, M.; Millam, J. M.; Klene, M.; Adamo, C.; Cammi, R.; Ochterski, J. W.; Martin, R. L.; Morokuma, K.; Farkas, O.; Foresman, J. B.; Fox, D. J. Gaussian~16 Revision C.01. 2016; Gaussian Inc. Wallingford CT.
- (33) Perdew, J. P.; Burke, K.; Ernzerhof, M. Generalized gradient approximation made simple. *Phys. Rev. Lett.* **1996**, *77*, 3865–3868, DOI: 10.1103/PhysRevLett.77.3865.
- (34) Adamo, C.; Barone, V. Toward reliable density functional methods without adjustable parameters: The PBE0 model. *J. Chem. Phys.* **1999**, *110*, 6158–6170, DOI: 10.1063/1.478522.
- (35) Grimme, S.; Antony, J.; Ehrlich, S.; Krieg, H. A consistent and accurate ab initio parametrization of density functional dispersion correction (DFT-D) for the 94 elements H-Pu. *J. Chem. Phys.* **2010**, *132*, 154104, DOI: 10.1063/1.3382344.
- (36) Grimme, S.; Ehrlich, S.; Goerigk, L. Effect of the damping function in dispersion

- corrected density functional theory. *J. Comput. Chem.* **2011**, *32*, 1456–1465, DOI: 10.1002/jcc.21759.
- (37) Küchle, W.; Dolg, M.; Stoll, H.; Preuss, H. Energy-adjusted pseudopotentials for the actinides. Parameter sets and test calculations for thorium and thorium monoxide. *J. Chem. Phys.* **1994**, *100*, 7535, DOI: 10.1063/1.466847.
- (38) Cao, X.; Dolg, M.; Stoll, H. Valence basis sets for relativistic energy-consistent small-core actinide pseudopotentials. *J. Chem. Phys.* **2003**, *118*, 487, DOI: 10.1063/1.1521431.
- (39) Cao, X.; Dolg, M. Segmented contraction scheme for small-core actinide pseudopotential basis sets. *J. Mol. Struct. (Theochem)* **2004**, *673*, 203–209, DOI: 10.1016/j.theochem.2003.12.015.
- (40) Weigend, F.; Ahlrichs, R. Balanced basis sets of split valence, triple zeta valence and quadruple zeta valence quality for H to Rn: Design and assessment of accuracy. *Phys. Chem. Chem. Phys.* **2005**, *7*, 3297–3305, DOI: 10.1039/B508541A.
- (41) Gutowski, K. E.; Dixon, D. A. Predicting the Energy of the Water Exchange Reaction and Free Energy of Solvation for the Uranyl Ion in Aqueous Solution. *J. Phys. Chem. A* **2006**, *110*, 8840–8856, DOI: 10.1021/jp061851h.
- (42) Wählin, P.; Danilo, C.; Vallet, V.; Réal, F.; Flament, J.-P.; Wahlgren, U. An investigation of the accuracy of different DFT functionals on the water exchange reaction in hydrated uranyl(VI) in the ground state and the first excited state. *J. Chem. Theory Comput.* **2008**, *4*, 569–577, DOI: 10.1021/ct700062x.
- (43) Austin, J. P.; Burton, N. A.; Hillier, I. H.; Sundararajan, M.; Vincent, M. A. Which density functional should be used to study actinyl complexes? *Phys. Chem. Chem. Phys.* **2009**, *11*, 1143–1145, DOI: 10.1039/b821577d.

- (44) Bader, R. F. W. A Quantum Theory of Molecular Structure and Its Application. *Chem. Rev.* **1991**, *91*, 893–928, DOI: 10.1021/cr00005a013.
- (45) Bader, R. F. W. *Atoms in Molecules - A Quantum Theory*; Oxford University Press, 1994.
- (46) Keith, T. A. AIMAll (version 19.10.12), Todd A. Keith, TK Gristmill Software: Overland Park KS, 2019. <http://aim.tkgristmill.com>.
- (47) Glendening, E. D.; Badenhop, J. K.; Reed, A. E.; Carpenter, J. E.; Bohmann, J. A.; Morales, C. M.; Karafiloglou, P.; Landis, C. R.; Weinhold, F. NBO 7.0. 2018.
- (48) Yanai, T.; Tew, D. P.; Handy, N. C. A new hybrid exchange-correlation functional using the Coulomb-attenuating method (CAM-B3LYP). *Chem. Phys. Lett.* **2004**, *393*, 51–57, DOI: 10.1016/j.cplett.2004.06.011.
- (49) Tecmer, P.; Bast, R.; Ruud, K.; Visscher, L. Charge-Transfer Excitations in Uranyl Tetrachloride ( $[\text{UO}_2\text{Cl}_4]^{2-}$ ): How Reliable are Electronic Spectra from Relativistic Time-Dependent Density Functional Theory? *J. Phys. Chem. A* **2012**, *116*, 7397–7404, DOI: 10.1021/jp3011266.
- (50) Tecmer, P.; Govind, N.; Kowalski, K.; de Jong, W. A.; Visscher, L. Reliable modeling of the electronic spectra of realistic uranium complexes. *J. Chem. Phys.* **2013**, *139*, 034301, DOI: 10.1063/1.4812360.
- (51) Oher, H.; Réal, F.; Vercouter, T.; Vallet, V. Investigation of the Luminescence of  $[\text{UO}_2\text{X}_4]^{2-}$  ( $\text{X} = \text{Cl}, \text{Br}$ ) Complexes in the Organic Phase Using Time-Resolved Laser-Induced Fluorescence Spectroscopy and Quantum Chemical Simulations. *Inorg. Chem.* **2020**, *59*, 5896–5906, DOI: 10.1021/acs.inorgchem.9b03614.
- (52) Oher, H.; Vercouter, T.; Réal, F.; Shang, C.; Reiller, P. E.; Vallet, V. Influence of alkaline earth metal ions on structures and luminescent properties of

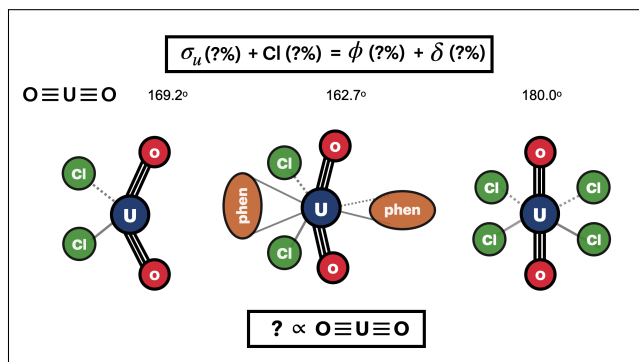
- $\text{Na}_m\text{Me}_n\text{UO}_2(\text{CO}_3)_3^{(4-m-2n)-}$  (Me = Mg, Ca; m, n = 0-2): time-resolved fluorescence spectroscopy and ab initio studies. *Inorg. Chem.* **2020**, *59*, 15036–15049, DOI: 10.1021/acs.inorgchem.0c01986.
- (53) Oher, H.; Ferru, G.; Couston, L.; Berthon, L.; Guillaumont, D.; Réal, F.; Vercouter, T.; Vallet, V. Influence of the first coordination of uranyl on its luminescence properties: study of uranyl binitrate with N,N-dialkyl amide DEHiBA and water. *Inorg. Chem.* **2022**, *61*, 890–901, DOI: 10.1021/acs.inorgchem.1c02618.
- (54) Yang, J.-J.; Zhao, Z.; Su, J. Theoretical Study of the Excited States and Luminescent Properties of  $(\text{H}_2\text{O})_n\text{UO}_2\text{Cl}_2$  (n = 1–3). *Inorg. Chem.* **2023**, *62*, 1978–1987, DOI: 10.1021/acs.inorgchem.2c03249.
- (55) Misael, W. A.; Gomes, A. S. P. Core excitations and ionizations of uranyl in  $\text{Cs}_2\text{UO}_2\text{Cl}_4$  from relativistic embedded damped response time-dependent density functional theory and equation of motion coupled cluster calculations. **2023**, arXiv:2302.07223 [physics.chem-ph], DOI: 10.48550/arXiv.2302.07223.
- (56) Fonseca Guerra, C.; Snijders, J. G.; te Velde, G.; Baerends, E. J. *Theor. Chem. Acc.* **1998**, *99*, 391–403, DOI: 10.1007/s002149800m26.
- (57) te Velde, G.; Bickelhaupt, F. M.; Baerends, E. J.; Fonseca Guerra, C.; van Gisbergen, S. J. A.; Snijders, J. G.; Ziegler, T. Chemistry with ADF. *J. Comput. Chem.* **2001**, *22*, 931–967, DOI: 10.1002/jcc.1056.
- (58) ADF2021.106. <http://www.scm.com>.
- (59) van Lenthe, E.; Baerends, E. J.; Snidjers, J. G. Relativistic regular two-component Hamiltonians. *J. Chem. Phys.* **1993**, *99*, 4597–4610, DOI: 10.1063/1.466059.
- (60) van Lenthe, E.; Baerends, E. J.; Snidjers, J. G. Relativistic total energy using regular approximations. *J. Chem. Phys.* **1994**, *101*, 9783–9792, DOI: 10.1063/1.467943.

- (61) van Lenthe, E.; Ehlers, A.; Baerends, E. J. Geometry optimizations in the zero order regular approximation for relativistic effects. *J. Chem. Phys.* **1999**, *110*, 8943–8953, DOI: 10.1063/1.478813.
- (62) Van Lenthe, E.; Baerends, E. J. Optimized Slater-type basis sets for the elements 1–118. *J. Comput. Chem.* **2003**, *24*, 1142–1156, DOI: 10.1002/jcc.10255.
- (63) Mozhayskiy, V.; Krylov, A. ezSpectrum, <http://iopenshell.usc.edu/downloads>. <http://iopenshell.usc.edu/downloads>.
- (64) Jin, J.; Gondalia, R.; Heaven, M. C. Electronic Spectroscopy of  $\text{UO}_2\text{Cl}_2$  Isolated in Solid Ar. *J. Phys. Chem. A* **2009**, *113*, 12724–12728, DOI: 10.1021/jp9052133.
- (65) Schnaars, D. D.; Wilson, R. E. Lattice Solvent and Crystal Phase Effects on the Vibrational Spectra of  $\text{UO}_2\text{Cl}_4^{2-}$ . *Inorg. Chem.* **2014**, *53*, 11036–11045, DOI: 10.1021/ic501553m.
- (66) Schnaars, D. D.; Wilson, R. E. Structural and vibrational properties of  $\text{U(VI)O}_2\text{Cl}_4^{2-}$  and  $\text{Pu(VI)O}_2\text{Cl}_4^{2-}$  Complexes. *Inorg. Chem.* **2013**, *52*, 14138–14147, DOI: 10.1021/ic401991n.
- (67) Sheldrick, G. M. SADABS, Program for Empirical Absorption Correction of Area Detector Data. 1996.
- (68) Sheldrick, G. M. A Short History of SHELX. *Acta Crystallogr. A* **2008**, *64*, 112–122, DOI: 10.1107/S0108767307043930.
- (69) Wadt, W. R. Why  $\text{UO}_2^{2+}$  is linear and isoelectronic  $\text{ThO}_2$  is bent? *J. Am. Chem. Soc.* **1981**, *103*, 6053, DOI: 10.1021/ja00410a011.
- (70) Tatsumi, K.; Hoffmann, R. Bent cis  $d^0$   $\text{MoO}_2^{2+}$  vs linear trans  $d^0f^0$   $\text{UO}_2^{2+}$ : A significant role for nonvalence 6p orbitals in uranyl. *Inorg. Chem.* **1980**, *20*, 1950, DOI: 10.1021/ic50211a035.

- (71) Su, J.; Dau, P. D.; Qiu, Y.-H.; Liu, H.-T.; Xu, C.-F.; Huang, D.-L.; Wang, L.-S.; Li, J. Probing the Electronic Structure and Chemical Bonding in Tricoordinated Uranyl Complexes  $\text{UO}_2\text{X}_3^-$  (X=F, Cl, Br, I): Competition between Coulomb Repulsion and U-X Bonding. *Inorg. Chem.* **2013**, *52*, 6617–6626, DOI: 10.1021/ic4006482.
- (72) Ruipérez, F.; Wahlgren, U. Charge transfer in uranyl(VI) halides  $[\text{UO}_2\text{X}_4]^{2-}$  (X = F, Cl, Br and I). A quantum chemical study of the absorption spectra. *J. Phys. Chem. A* **2010**, *114*, 3615–3621, DOI: 10.1021/jp911271q.
- (73) (a) Dreuw, A.; Head-Gordon, M. Failure of Time-Dependent Density Functional Theory for Long-Range Charge-Transfer Excited States: The Zinbacteriochlorin-Bacteriochlorin and Bacteriochlorophyll-Spheroidene Complexes. *J. Am. Chem. Soc.* **2004**, *126*, 4007–4016, DOI: 10.1021/ja039556n; (b) Eriksen, J. J.; Sauer, S. P.; Mikkelsen, K. V.; Christiansen, O.; Jensen, H. J. A.; Kongsted, J. Failures of TDDFT in describing the lowest intramolecular charge-transfer excitation in para-nitroaniline. *Mol. Phys.* **2013**, *111*, 1235–1248, DOI: 10.1080/00268976.2013.793841.
- (74) Wang, Z.; M. Zachara, J.; Liu, C.; Gassman, P.; R. Felmy, A.; B. Clark, S. A cryogenic fluorescence spectroscopic study of uranyl carbonate, phosphate and oxyhydroxide minerals. *Radiochim. Acta* **2008**, *96*, 591–598, DOI: 10.1021/es048448d.
- (75) Denning, R. G.; Snellgrove, T. R.; Woodwark, D. R. The electronic structure of the uranyl ion: Part I. The electronic spectrum of  $\text{Cs}_2\text{UO}_2\text{Cl}_4$ . *Mol. Phys.* **1976**, *32*, 419–442, DOI: 10.1080/00268977600103211.
- (76) Leszczyk, A.; Dome, T.; Tecmer, P.; Kedziera, D.; Boguslawski, K. Resolving the  $\pi$ -assisted U–N  $\sigma_f$ -bond formation using quantum information theory. *Phys. Chem. Chem. Phys.* **2022**, *24*, 21296–21307, DOI: 10.1039/D2CP03377A.
- (77) Oher, H.; Gomes, A. S. P.; Wilson, R. E.; Schnaars, D. D.; Vallet, V. How does bending

the uranyl unit influence its spectroscopy and luminescence. **2023**, ChemRxiv, DOI:  
10.26434/chemrxiv-2023-m3spw-v2.

## TOC Graphic



The luminescence spectrum of a bent uranyl complex with chloride ligands and 1,10-phenanthroline ligands has been experimentally recorded for the first time, and also successfully computed by vibrationally resolved ab initio calculations. Notably, we demonstrate that the bending of uranyl in  $\text{UO}_2\text{Cl}_2(\text{phen})_2$  and in the  $\text{UO}_2\text{Cl}_2$  complex triggers vibronically induced excitations of the uranyl bending mode, yielding denser luminescence spectra than in linear uranyl complexes.